Wall Functions for Incorporation of Atomistic Physics into Continuum Modeling of Electrokinetic Flow

R. H. Nilson* and S. K. Griffiths**

Physical and Engineering Sciences Center
Sandia National Laboratories
P. O. Box 969, Livermore CA 94551, USA
*rhnilso@sandia.gov **skgriff@sandia.gov

ABSTRACT

Wall functions derived from Density Functional Theory (DFT) are used to incorporate non-continuum atomistic physics into continuum modeling of electroosmotic flow in slit-like channels ranging in width from a few molecular diameters to scales several orders greater. These wall functions represent deviations of the electrochemical potentials of charged and uncharged species from their nominal continuum values due to Lennard-Jones interactions among fluid and solid molecules, hard sphere repulsions, and short range non-coulombic electrical interactions. Because these deviations decrease strongly with distance from the charged surfaces, the wall functions computed for a channel width of 10 or more molecular diameters can be applied to all wider channels. Electroosmotic speeds computed by this DFT-based approach are sometimes two or three times smaller than those predicted by more primitive Poisson-Boltzmann modeling, particularly for large surface charge densities, large electrolyte concentrations, and small channel sizes.

Keywords: electroosmotic flow, nanofluidics, microfluidics, wall functions, electrophoresis

1 INTRODUCTION

The atomistic physics of fluid/solid interfacial layers may substantially influence fluid flow and ion transport, particularly in nanoscale channels. As illustrated in Figures 1 and 2, interfacial fluid molecules are ordered by the planar structure of adjacent solid surfaces. Within the first monolayer, the local density of molecular centers is typically several times greater than that of a homogeneous far-field fluid. Successive density peaks, spaced roughly one molecular diameter apart, become progressively weaker with increasing distance from the surface. These local density variations alter the fluid viscosity, reduce ion diffusivity, and alter the distribution of the electrical body forces that control the speed of electroosmotic flows.

Previous studies addressing non-continuum fluid mechanics have been largely based on Molecular Dynamics (MD) simulations [1]. Although these models directly treat the atomistic physics of interest, they often require long computing times and are not readily integrated into traditional continuum modeling tools needed to address complex multiscale systems of engineering interest.

In the present paper we use Density Functional Theory (DFT) [2] to compute fluid and ion density profiles within slit-like channels. From these results we determine wall functions describing deviations of the electrochemical potential from nominal continuum values as a function of distance from the channel walls. It is shown that these wall functions are relatively insensitive to channel size for widths greater than a few molecular diameters. Finally, the wall functions are used in conjunction with the governing Poisson equation, ion transport equations, and Navier Stokes equations to compute electroosmotic velocity profiles in channel sizes ranging over several orders of magnitude.

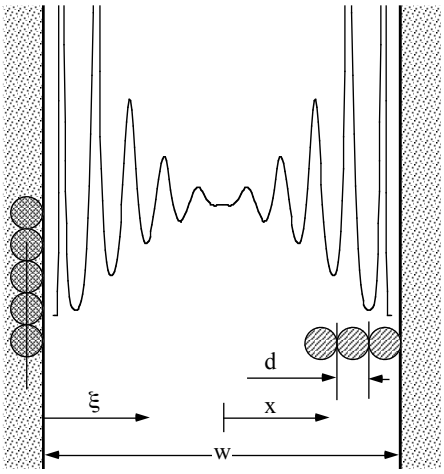

Figure 1: Density profile of an uncharged liquid in a narrow slit. Density of molecular centers is greatest in layers adjacent to planar walls. Peaks are spaced one molecular diameter apart.

2 GOVERNING EQUATIONS

We restrict our attention to steady fully-developed electroosmotic flow of an incompressible liquid in a slit-like channel with the x and z coordinates directed across and along the channel, respectively. Under these conditions the transverse velocity components, u_x and u_y, vanish, and

the dependent variables become independent of axial position. The momentum equation then takes the following form [3]

$$\frac{\partial}{\partial x}\left(\mu\frac{\partial u}{\partial x}\right) = -\rho_e\frac{\partial\phi}{\partial z} \equiv -\rho_e E_z \qquad (1)$$

where $u \equiv u_z(x)$ is the axial fluid flow speed, ϕ is the electric potential, ρ_e is the local charge density, and E_z is the applied axial electric field. The electric potential is related to the charge distribution by the Poisson equation

$$\varepsilon\,\nabla^2\phi = -\rho_e \qquad (2)$$

where ε is the permittivity of the liquid. The local charge density appearing in the momentum balance and in Poisson's equation is obtained by summing the contributions from the N molecular species. Densities of the individual ion species, ρ_i, are generally determined by solving species conservation equations of the form [3]

$$\nabla\cdot\left(\rho_i\mathbf{u} - \upsilon_i\,\rho_i\nabla\gamma_i\right) = 0 \qquad (3)$$

Here, γ_i is the electrochemical potential and υ_i is the species mobility related to the dilute species diffusivity, D_i, through the Nernst-Einsten equation, $\upsilon_i = D_i/kT$.

In classical continuum models, the chemical potential of a species is generally assumed to depend on the logarithm of the species density and the potential energy relative to the electric field [3]

$$\gamma_i = \gamma_i^0 + kT\ln\rho_i + z_i e\phi \qquad (4)$$

where γ_i^o is a reference potential, k is Boltzmann's constant and T is the temperature.

In Density Functional Theory, minimization of the Helmholtz free energy yields an expression of the following form for the chemical potential of each species [2].

$$\gamma_i = \gamma_i^0 + kT\ln\rho_i + z_i e\phi + \delta f_i^{elec} + f_i^{LJ} + f_i^{hs} + v_i \qquad (5)$$

The first three terms are identical to those of the classical theory in Eq. (4). The fourth term, δf_i^{elec}, represents the deviation of short range electrical interactions from the classical columbic model; it is modeled here using the mean field spherical approximation (MSA) derived by Waisman and Lebowitz. Attractive energies are defined by a density weighted integral of a pair potential function, $u_{ij}(s)$, over the surrounding fluid, separately summing the contributions from each species.

$$f_i^{LJ}(\mathbf{r},\{\rho\}) = \sum_j \int \rho_j(\mathbf{r}')\; u_{ij}(s)\, d\mathbf{r}' \qquad (6)$$

Here $s = |\mathbf{r} - \mathbf{r}'|$ and $u_{ij}(s)$ is taken as a cut and shifted version the Lennard-Jones (LJ) 6-12 potential. Hard sphere repulsions among fluid molecules, f_i^{hs}, are modeled using the highly successful Tarazona model. Finally, the external potential, v_i, is obtained by summing LJ interactions over planar sheets of atoms typical of an fcc solid.

The DFT equations are solved on a discretized spatial grid by iteratively adjusting the local densities of each species to satisfy Eq. (5) at all points for all species. The electric field is simultaneously computed from Eq. (2) using most recent values of the DFT charge distribution. Once the DFT solutions are converged, it is a simple manner to extract the wall functions, $\Delta\gamma_i(\xi)$, representing the deviation of the local DFT chemical potential from the classical model as a function of distance, ξ, from the surface.

$$\Delta\gamma_i(\xi) \equiv \gamma_{DFT} - \gamma_{classical} = \delta f_i^{elec} + f_i^{LJ} + f_i^{hs} + v_i \qquad (7)$$

The first term describing short range electrical interactions applies only to ion species, while the other three terms apply to all species.

The wall functions, so determined, can be used in two alternative manners. In multidimensional applications, the wall functions can be added to the chemical potential used in solving the generalized transport equation, Eq. (3). However, in the present channel flow problem and others like it, the transverse velocity is zero, or negligible, within the few molecular layers adjacent to the surface. Under this relatively weak restriction, Eq. (3) requires that the electrochemical potential of each ion species must be uniform within the surface layer and, hence, Eqs. (4,5) yield a modified Boltzmann equation for the ion distributions.

$$\frac{\rho_i(\xi)}{\rho_i^o} = \exp\left(-\frac{z_i\, e\left(\phi(\xi) - \phi^o\right) + \Delta\gamma_i(\xi)}{kT}\right) \qquad (8)$$

A similar correction to the Boltzmann equation was deduced from MD simulations by Qiao and Aluru in [1]. Once the wall functions are known, they can be used in conjunction with the usual governing equations, (1-3), to compute electroosmotic flows in the same manner as done in conventional continuum codes. Moreover, since the wall functions are relatively insensitive to the channel width, a single set of wall functions can be applied to problems on a wide range of domain sizes. This is particularly beneficial on large domains, because it eliminates the need for fine DFT gridding over large regions.

3 EXAMPLE CALCULATIONS

All of our example calculations utilize a three component model having solvent, coion, and counterion species. All three species have a molecular diameter of d=4.25 A^o, the

temperature is 298 K, and the dielectric constant, ε*=78.5, is assumed to be the same for the fluid and the adjacent solid, thus eliminating the need for image charges. The corresponding value of the plasma constant, $\beta^* = e^2/\varepsilon kTd$, is 1.68. The bulk molecular density of the solvent is $\rho_\infty = 0.7/d^3$, and the LJ potential well depth is $\varepsilon^{LJ} = kT$ for all species. In addition, the ion concentrations of the reference state (eg. a large reservoir connected to the channel) will be varied from C_∞=0.001 to 1.0 moles/liter.

Figure 2 illustrates ion density profiles computed by DFT (symbols) and by the classical Poisson-Boltzmann (PB) model (dotted) lines. To accentuate differences between the models, the normalized surface charge density has been taken at the upper end of the range normally encountered in microfluidic devices, $\sigma^* = \sigma d^2/e$=0.5. It is seen that the DFT model tends to shift more of the counterions toward the charged surface, relative to PB. This is partly because of the layering phenomenon seen earlier in Fig. 1, and partly because the electrical interactions among like charges are weakened by the short range MSA corrections to the classical coulombic model. Further, since the integral of the charge distribution must be identical to the prescribed surface for both solutions, the PB solution has a greater concentration of counterions in the channel center.

This shifting of counterions toward the channels walls reduces the effective thickness of the Debye layer, increases the viscous shear stresses, and reduces the electroosmotic speed of the DFT solutions, compared to PB. The disparity in the normalized mean speed, averaged over the channel width, is illustrated in Fig. 3 as a function of the channel width. The disparity between DFT and PB speeds increases with increasing surface charge density and with decreasing channel size. The latter influence is partly due to a difference in the location of the no-slip boundary condition. In both cases, the boundary condition is applied at the position of closest approach of charged ions. For DFT this position is one half molecular diameter from the outer edge of the wall molecules, whereas in classical PB the charge density is actually greatest immediately adjacent to the surface so, in classical PB, the no-slip condition is applied at the surface.

Wall functions computed from DFT solutions in accordance with Eq. (7) are illustrated in Fig. 4 for four different choices of the normalize channel width. The electrical portions of the wall functions, δf_i^{elec}, having opposite signs for the oppositely charged ions species are essentially independent of the channel width for w*=w/d>3 because their magnitude becomes relatively small within two molecular diameters of the surface. The oscillatory portion of the wall functions, applicable to all species, is mainly a consequence of the layered ordering induced by the planar channel wall illustrated earlier in Figs. 1 and 2. This phenomenon is longer ranged and thus more sensitive to the channel width. Even so, the wall functions for a channel width of w*=10 can certainly be applied to all wider channels.

However, it is somewhat surprising and encouraging to find that wall functions calculated from the DFT results for w*=10 can also be applied to narrower channels as well as wider ones. This is demonstrated in Fig. 3 by comparison of exact DFT results (symbols) for various channel widths with approximate solutions obtained by solving Eqs. (1,2,8) using

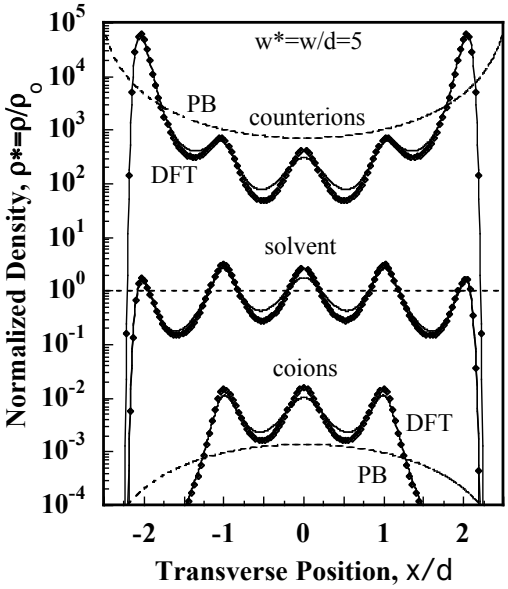

Figure 2: Comparison of ion density profiles computed by DFT (symbols), classical Poisson-Boltzmann theory (dotted), and by wall functions based on DFT solutions for w*=10 (solid lines). C_∞=0.001 M, σ*=0.5.

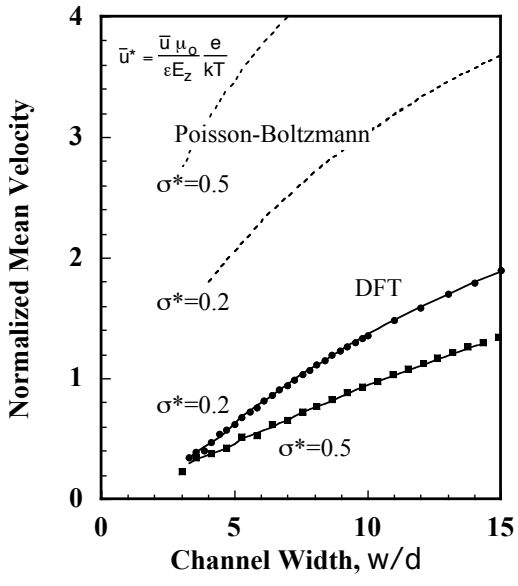

Figure 3: DFT (symbols) predicts smaller speeds than classical PB (dotted). Speeds based on wall functions for w*=10 (solid lines) are in excellent agreement with full DFT solutions (symbols). C_∞=0.001 M.

wall functions, $\Delta\gamma_i(\xi)$, computed from the DFT results for w*=10. The two sets of results are nearly indistinguishable over the full range of channel widths from w*=3 to 15. A similar comparison is made in Fig. 2 where the exact DFT results for ion and solvent density profiles (symbols) in a channel of width w*=5 are compared with approximate results (solid lines) based again on wall functions for w*=10. The agreement is quite good, even for the solvent molecules, despite the fact that the solvent is only influenced by the longer ranged steric component of $\Delta\gamma_i(\xi)$.

Figure 5 compares mean electroosmotic speeds computed by the classical Poisson Boltzmann approach (dotted) with results obtained using wall functions based on DFT solutions for a channel width of w*=10 (symbols and solid lines). Although the PB solutions depend on the concentration, C_∞, this dependence is eliminated from Fig. 5 by plotting the speed versus the normalized Debye thickness, λ, which is inversely proportional to the square root of C_∞. In contrast, the DFT-based wall function results still do depend on C_∞, in spite of this scaling of the plot.

For each of the molarities indicated in Fig, 5, the DFT symbol furthest to the right in each line is for a channel width of w*=3. However, owing to the inverse square root dependence of λ on C_∞, the corresponding values of λ /w decrease from 15, to 1.5, to 0.47 as C_∞ increase from 0.001, to 0.1, to 1.0 M. Rather than prescribing the surface charge density, as in previous examples, the surface potential is now prescribed as $\zeta^* = \zeta e/kT = 2$. For this modest zeta potential, the PB model provides good results for 0.001 M. However, deviations become large for C_∞= 0.1 and 1.0 M, particularly for the smaller channels. At larger zeta, the deviations between DFT and PB grow even larger.

4 SUMMARY

Wall functions derived from DFT have been used to compute electroosmotic flows in a broad range of channel sizes. A single set of wall functions computed for a channel size of w*=w/d=10 appears applicable to all channel widths w*>3. Comparison of these DFT-based results with classical Poisson-Boltzmann modeling indicates that PB may be substantially in error when channel sizes are small, molarities are large, and surface charge density or zeta potential are relatively large.

REFERENCES

[1] R. Qiao and N. R. Aluru, "Ion concentrations and velocity profiles in nanochannel electroosmotic flows", J. Chem Phys., 104, (3) 268, 2003.

[2] Z. Tang, L. Mier-Y-Teran, H. T. Davis, L. E. Scriven, and H. S. White, "Non-local free-energy density functional theory applied to the electric double layer,", Molecular Physics 71 (2) 369, 1990.

[3] R. F. Probstein, Physicochemical Hydrodynamics, Wiley-Interscience, New York, 1994.

*Sandia is a multiprogram laboratory operated by Sandia Corporation, a Lockheed Martin Company, for the United States Department of Energy's National Nuclear Security Administration under contract DE-AC04-94AL85000.

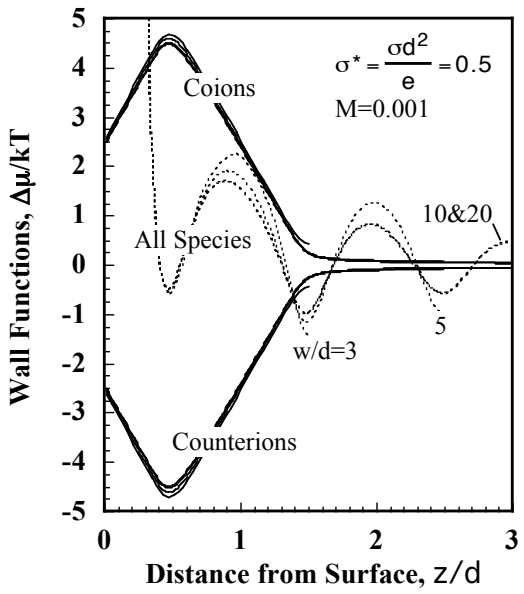

Figure 4: Wall functions depend only weakly on channel width, w. Oscillatory repulsions (dotted) apply to all species. Additive electrical contributions (solid) apply to singly-charged coions and counterions.

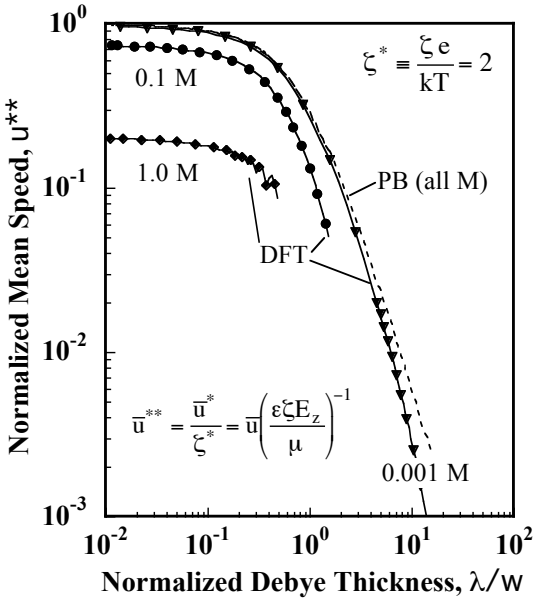

Figure 5: Comparison of DFT wall function results (symbols) with classical PB solutions (dotted line) for fixed surface potential and various concentrations. Speeds are normalized by the prescribed surface zeta potential.